Photoconducting state and its perturbation by electrostatic fields in oxide-based two-dimensional electron gas

A. Rastogi,[1] J. J. Pulikkotil,[2] S. Auluck,[2] Z. Hossain,[1] and R. C. Budhani[1,2,*]

[1]*Condensed Matter Low Dimensional Systems Laboratory, Department of Physics, Indian Institute of Technology, Kanpur 208016, India*

[2]*National Physical Laboratory, Council of Scientific and Industrial Research, Dr. K. S. Krishnan Marg, New Delhi 110012, India*

(Received 25 June 2012; published 16 August 2012)

The two-carrier transport model as proposed for the two-dimensional electron gas formed at the interfaces of oxide heterostructures is investigated by means of a combined perturbation by near-ultraviolet radiation and an electrostatic field, applied both separately and simultaneously. Comparison of the photoresponse of prototype systems such as the band insulator $LaAlO_3$ and Mott insulator $LaTiO_3$ films on TiO_2-terminated $SrTiO_3$ shows remarkably similarities. Two types of nonequilibrium carrier are generated in each system, each having the signature of a particular type of perturbation characterized by distinctly different relaxation processes. While the photoconducting state diminishes in a stretched exponential manner, with a temperature-dependent activation energy varying from a few tens of meV to $\approx$1 to 2 meV on lowering the temperature and a relaxation time of several hours, the recovery from electrostatic gating occurs on the millisecond time scale. An attempt is also made to explain the experimental observations using *ab initio* density functional calculations. The calculations show that the electronic transitions associated with near-ultraviolet radiation emerge from bands located at $\simeq$2 eV above and below the Fermi energy, which are the Ti 3*d* states of the $SrTiO_3$ substrate and of the AlO_2 (TiO_2) layers of the $LaAlO_3$ ($LaTiO_3$) films, respectively. The slow decay of the photocurrent to the unperturbed state is explained in terms of the closely spaced Ti $3d_{xy}$ states in the lower conduction band, which are manifested as flatbands (or localized states) in the band structure. Such localization leads to increased carrier lifetimes, through the energy-time relationship of the uncertainty principle.

DOI: 10.1103/PhysRevB.86.075127 PACS number(s): 73.40.−c, 73.20.At, 74.25.F−, 78.66.−w

I. INTRODUCTION

Polarization discontinuity at the interface of oxide heterostructures, such as that of $LaAlO_3$ or $LaTiO_3$ on TiO_2-terminated $SrTiO_3$, induces a large in-built electric field.[1,2] This thermodynamic instability is nullified by one or more mechanism(s) such as atomic relaxation,[3] electronic reconstruction,[4,5] interlayer cation mixing,[6,7] and/or creation of vacancies,[8,9] thereby resulting in the formation of a two-dimensional electron gas (2DEG).[1,10–12] The properties of such a 2DEG state have been extensively studied in the recent past, owing to its display of magnetism, superconductivity, and the fractional quantum Hall effect.[8,9,13–18] Thus, the subject of addressing the origin and nature of these charge carriers has captured much attention. Brinkman *et al*. propose that the 2DEG comprises two different types of charge carrier, which fundamentally allows for the coexistence of two order parameters, namely, superconductivity and magnetism,[15] with the latter being associated with the localized electrons of the Ti 3*d* orbitals and superconductivity being mediated via the itinerant electrons. A two-band model has been proposed to describe the dependence of the sheet resistance and Hall coefficient under the influence of a magnetic field.[19] The two-carrier model is also supported by means of density functional calculations[20,21] and high-field Hall measurements.[22] There is also evidence both for and against a multiband model with two electron populations to describe the transport at the oxide interfaces.[23–25] Beyond this, it has also been observed that the properties exhibited by the 2DEG at the interfaces can be altered by an electrostatic potential applied in a field-effect geometry.[17,26–30]

From the electronic transport perspective, films of $LaAlO_3$ (LAO) and $LaTiO_3$ (LTO) grown on TiO_2-terminated $SrTiO_3$ (STO) substrates with film thickness of 20 Å ($\simeq$4 unit cells) and above show a sheet carrier density of $\sim 10^{13}$ cm^{-2}.[8,9,15–17] These values are significantly lower as compared to that reported in the original work of Ohtomo and Hwang,[1] which is $\sim 10^{17}$ cm^{-2}. The discrepancy seems to arise from the synthesis techniques, involving growth temperature and oxygen pressure during the growth of the films. While high carrier densities are associated with oxygen vacancies which are the source of the extra electrons, the state of reduced carriers appears as an intrinsic property of atomically abrupt interfaces. For such carrier-deficient systems, time-resolved photoluminescence experiments[30,31] have shown a pronounced photoconductivity activated by photons of wavelength $\lambda \leqslant 400$ nm. The ultraviolet-sensitive enhancement in conductivity has many characteristics that are similar to those seen in III-IV compound semiconductor interfaces such as GaAlAs/GaAs,[32,33] InGaP/GaAs,[34]and GaAlN/GaN.[35] In addition, a remarkable feature of the photoconductivity in these oxide heterostructures is their inordinately slow recovery to the unperturbed state on extinguishing the photoillumination.

Due to the inherent ability of transition-metal ions to display multivalent states, defects in the form of O vacancies would lead to electronic reconstruction in their neighborhood to preserve charge neutrality. If such a scenario leads to vacancy-derived localized states, they will serve as centers for optical excitations. If the centers are singly charged they act as recombination centers for minority carriers, while those which are doubly (or multiply) charged become traps.[36] However, in these oxide heterostructures it is observed that trapping centers exist even in the case of abrupt interfaces,[30] thereby suggesting a mechanism different from that of the defect-mediated centers. *Ab initio* calculations carried out

for fully relaxed abrupt interfaces reveal a series of closely spaced Ti $3d_{xy}$ states in the lower conduction band. These states, which are derived from the STO substrate, are highly localized and therefore tend to act as traps due to their increased carrier lifetimes. The above conclusion is derived from the energy-time relationship of the uncertainty principle. Beyond this, our finding that the change in resistance due to the electric field is independent of the recovery of the photoconducting state confirms that that the radiation and electric fields act on two different sources of carriers, and thus are partly decoupled in these heterostructures.

II. EXPERIMENTAL AND COMPUTATIONAL DETAILS

A. Experiments

Ultrathin films of LAO and LTO were deposited on (001)-cut STO single-crystal substrates by ablating well-sintered targets of these materials with nanosecond pulses of an excimer laser (KrF, $\lambda = 248$ nm). It has been shown that the properties of such films depend strongly on growth conditions, and a metallic interface is realized in films deposited on TiO_2-terminated surfaces. We achieved such termination by etching the substrate in buffered HF solution followed by cleaning in deionized water and alcohol for 20 min. The substrate was annealed at 800 °C for one hour in 7.4×10^{-2} mbar of oxygen to get a defect-free surface. LTO and LAO films of thickness 8 nm were deposited at 700, 750, and 800 °C in 1×10^{-4} mbar of O_2 at a slow rate (~0.12 Å/s) to realize a layer-by-layer growth. The films were cooled under the same pressure at the rate of 10 °C/min. Two sets of samples are used for the measurements; in one case 2.5×5 mm^2 slabs were prepared for standard four-probe measurements of resistance and photoconductivity by depositing Ag/Cr contact pads through a shadow mask such that the separation between voltage pads is ≃700 μm. For field-effect measurements, we have used 5×5 mm^2 samples. Here the source and drain were deposited to give an effective channel area of 200×100 μm^2, whereas the gate electrode was coated on the back side of the 0.5-mm-thick STO substrate. The integrated UV intensity ≃8 μW cm^{-2} of a quartz halogen lamp and He-Cd laser lines of 441 and 325 nm were used for photoillumination while the sample was mounted in a closed-cycle helium cryostat.

B. Theoretical calculations

On the theoretical front, the calculations were carried out using the full-potential linearized augmented plane-wave (FP-LAPW) method, as implemented in the WIEN2K suite of programs.[37] The LAO/STO heterostructures were modeled by stacking five unit cells of STO (representing the substrate) with four unit cells of LAO (representing the film), with cell dimension being that of STO ($a = 3.905$ Å). The structural parameters were fully relaxed using the force optimization technique. The exchange-correlation potential was described in the generalized gradient approximation (GGA). Convergence in the basis set was achieved with $RK_{max} = 6.0$, with R being the smallest LAPW sphere radius and K_{max} being the interstitial plane-wave cutoff. The sphere radii, in Bohr units, for Sr/La, Ti/Al, and O were chosen as 2.2, 1.9, and 1.6, respectively. Convergence of the Brillouin zone (BZ) sampling is attained for a Monkhorst-Pack k mesh of 90 k points in the irreducible region of the BZ.

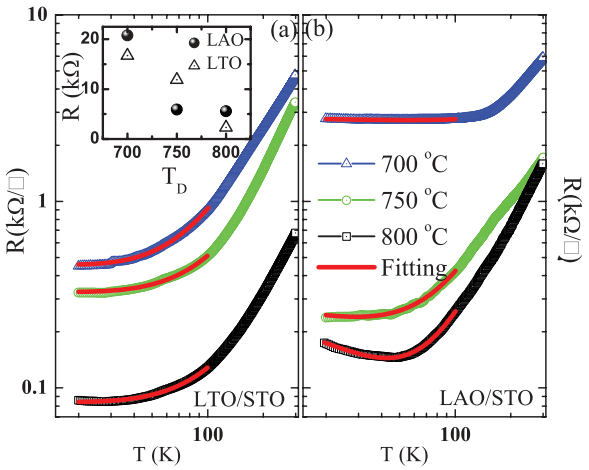

FIG. 1. (Color online) Temperature dependence of the sheet resistance down to 20 K for 8-nm-thick LTO/STO (a) and LAO/STO (b) films deposited at 700, 750, and 800 °C on a STO (001) substrate. Solid (red) lines are fitted to the expression $R = R_0 + AT^2 + B\ln T$, where R_0, A, and B are constants, over the temperature range 20 to 100 K. For LTO/STO, $B = 0$. A comparison of the room-temperature sheet resistance of LTO and LAO films as a function of growth temperature is shown in the inset of (a).

III. RESULTS AND DISCUSSION

A. Electrical transport

We first compare the sheet resistance (Ω/□) of LAO and LTO films grown at 700, 750, and 800 °C on the TiO_2-terminated STO substrate. The data shown in Figs. 1(a) and 1(b) are plotted on a logarithmic scale to emphasize the temperature dependence down to 20 K. The temperature dependence of resistance measured between 300 and 20 K shows metallic behavior for all films. The metallicity becomes robust for the films grown at higher temperatures. It is also interesting to note that while the sheet resistance of LAO/STO tends to saturate or even grow marginally below ≈50 K, the resistance of LTO/STO films continues to drop down to 20 K. The temperature dependence of the resistance of LTO/STO systems can be expressed as $R = R_0 + AT^2$, whereas for LAO/STO, a $B\ln T$ term needs to be added, where B is a negative coefficient. As evident from the inset of Fig. 1(a), the room-temperature resistance is less for LTO/STO than for the LAO/STO systems synthesized at 800 °C. With the structural symmetry and lattice parameters of both $LaTiO_3$ and $LaAlO_3$ being similar and because they have ≈2% of lattice mismatch with $SrTiO_3$, the difference in $R(T)$ may be attributed to the nature of electronic interactions in the films. We note that while $LaTiO_3$ is a Mott insulator, $LaAlO_3$ is a band insulator. Therefore, it may be inferred that the Ti $3d$ electrons, which are strongly correlated in $LaTiO_3$, play an important role in the low-temperature transport properties. It is also interesting to note that these films become superconducting, at lower temperatures ($T < 300$ mK).[18]

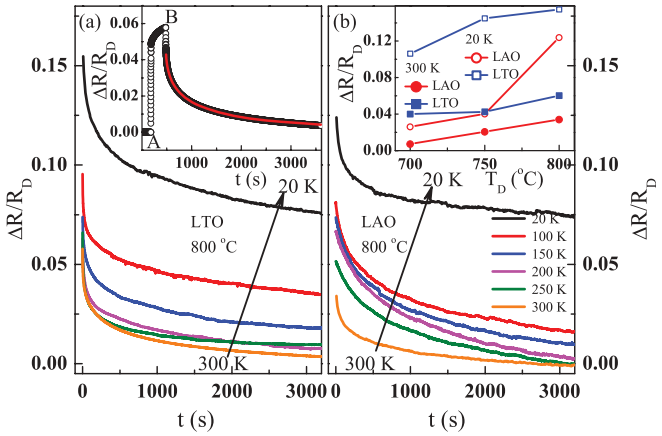

FIG. 2. (Color online) Temporal evolution of the normalized resistance $\Delta R/R_D$, as defined in text, after turning off the light, for 800 °C–deposited LTO/STO (a) and LAO/STO (b) films at different temperatures. The inset of (a) defines the instant at which the UV exposure was initiated and extinguished. At point A the exposure is switched on; at B it is turned off and the resistance is monitored as a function of time. The main panel shows the normalized resistance after point B. The inset of (b) shows the growth-temperature dependence of the maximum relative change in resistance for both the heterostructures at 20 and 300 K.

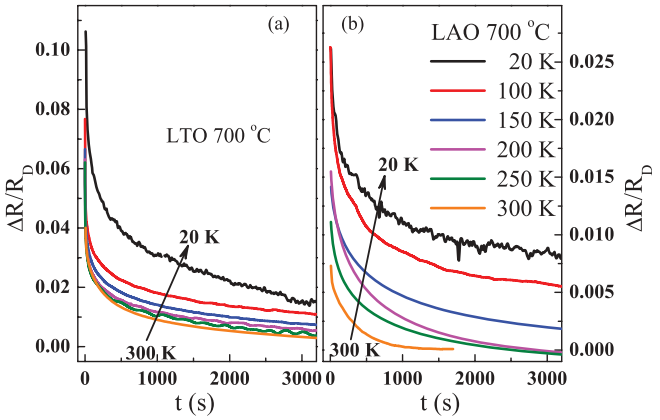

FIG. 3. (Color online) Time evolution of the normalized resistance at several temperatures for (a) LTO/STO and (b) LAO/STO deposited at 700 °C. The change in resistance in the case of LTO films is larger than that for the LAO. For both the films deposited at 700 °C the magnitude of the photoresponse is less than that seen in films deposited at 800 °C.

B. Photoconductivity

The resistance of LTO and LAO films shows nearly similar photoconductive behavior on exposure to the light from a quartz halogen lamp and also shows a similar decay behavior after removing the exposure. Using He-Cd laser of wavelengths 441 and 325 nm, we have further established that the photoconductivity emanates only from the UV component of the halogen lamp. The inset of Fig. 2(a) shows the temporal dependence of the change in resistance $\Delta R/R_D$, where $\Delta R = R_D - R(t)$, R_D is the resistance just before the exposure (point A in the figure), and $R(t)$ is the resistance at time t. The light of UV intensity $\approx 8\ \mu W/cm^{-2}$ is turned off at point B and the isothermal recovery of resistance is monitored as a function of time. The main panel of Fig. 2(a) shows the isothermal decay of the photoconducting state of the LTO film deposited at 800 °C. A similar set of data taken at different temperatures for the LAO film is shown in Fig. 2(b). The absolute value of $\Delta R/R_D$ just before extinguishing the exposure [corresponding to the point B in Fig. 2(a) inset] at 300 and 20 K for films grown at three different temperatures is plotted in the inset of Fig. 2(b). We note a distinctly larger change in the resistance of LTO films on photo exposure.

In Fig. 3 we compare the decay of the photoconducting state in the films deposited at 700 °C. From these data and also from the inset of Fig. 2(b) it is clear that the photoresponse is higher in LTO films irrespective of the growth temperature. This observation suggests that the intrinsic tendency of LTO to oxidize takes away oxygen from the substrate, rendering it photosensitive.

C. The Kohlrausch model

The time-dependent normalized resistance was fitted to the stretched exponential given by Kohlrausch;[38] $\frac{\Delta R(t)}{R_D} \sim \exp[-(\frac{t}{\tau})^{\beta}]$, where τ is the relaxation time constant and β the decay exponent, which takes values between 0 and 1.[38–40] The $\beta = 1$ situation describes the Debye relaxation process where a single activation energy is involved. A semilogarithmic plot of the time constant τ as a function of $(1/T)$ for the films grown at three different temperatures is shown in Fig. 4 along with the behavior of β. We note that the system recovers much faster at the higher temperatures of measurement. The exponent β also approaches a Debye-like behavior ($\beta = 1$) from the very small value of $\simeq$0.2 at 20 K. The $\ln(\tau)$ vs $(1/T)$ plot suggests a thermally activated behavior $\tau \sim \tau_0 \exp[-\frac{\Delta U}{k_B T}]$ where ΔU is a function of temperature and k_B the Boltzmann constant. A simplified picture of the recovery can be presented based on two activation energies as shown in Figs. 4(e) and 4(f). The energy changes from $\approx$1 to 11 meV as we go from the low-temperature to the high-temperature regime for the LTO system, while it ranges from $\approx$1 to 20 meV for the LAO system. This order of magnitude difference in $U(T)$ at low and high temperatures suggests a different dynamics of the migration of photoexcited carriers.

The two different regions in the Arrhenius plot [Figs. 4(e) and 4(f)] can be explained within the framework of the large lattice relaxation model[41] proposed earlier to understand the recovery from the photoconductive state in III-V compound semiconductors.[41,42] This model states that the photoconductivity decay is dominated by thermal activation of carriers to overcome the electron-capture barrier in the higher-temperature region, while at low temperatures the capture occurs by tunneling via multiphonon processes.[42,43] A similar argument could well be applied in the present case for the oxide heterostructures. However, it is interesting to note that the photoresponse in the LTO/STO and LAO/STO systems shows a significant drop on decreasing the growth temperature, with the response remaining sensitive to UV radiation only. In this context we emphasize that with increasing growth temperature, defects in the form of O vacancies may be created in the STO substrate just below the interface, driving

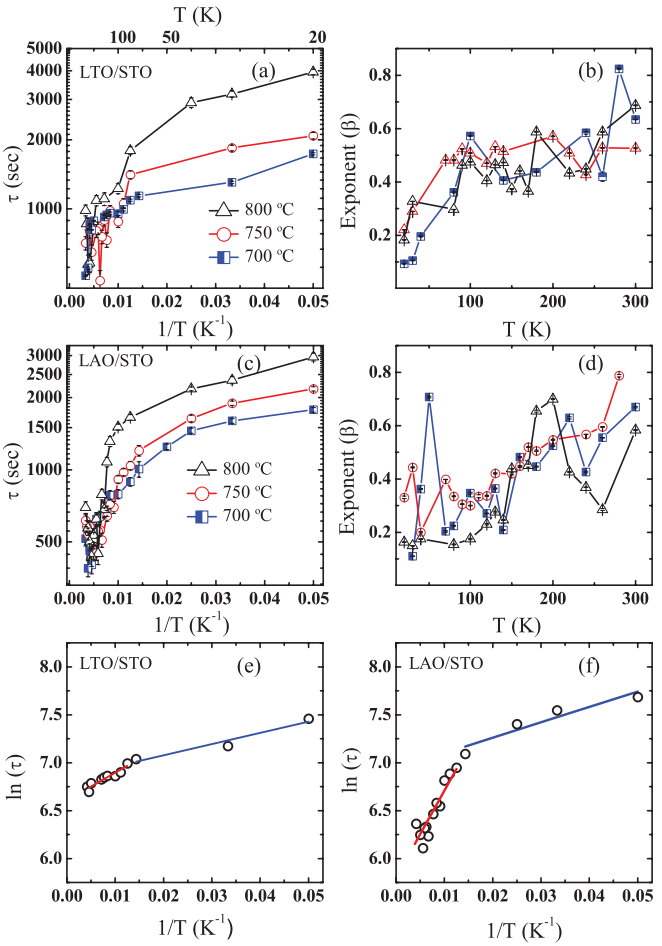

FIG. 4. (Color online) Critical parameters τ and β of the Kohlrausch expression for the LTO/STO and LAO/STO systems. The variation of the time constant with $1/T$ is plotted on a semilogarithmic scale in (a) and (c) for LTO/STO and LAO/STO films, respectively, grown at different T_D. The dependence of the exponent is plotted in (b) and (d), respectively. The values of τ and β were extracted from fitting the photoresponse at different temperatures to the Kohlrausch expression. The temperature dependence of the time constant can be fitted to the Arrhenius equation with two different activation energies as shown in (e) and (f).

the interfacial Ti ions to exhibit multivalent states. Isolated oxygen vacancies in STO imply a $3d^1$ configuration of Ti in its neighborhood, whose scattering cross section would be very different from that of a Ti ion with $3d^0$ electronic configuration. Thus defect-induced localized states, which are prominent in samples grown at high temperatures are expected to have more traps as compared to the samples with abrupt interfaces grown at low temperatures. This suggests that the decay of UV-generated photocurrent can be precisely controlled by varying the growth conditions of the sample. The value of τ at 20 K varies from ~3950 to 1750 s and from ~2955 to 1700 s for LTO/STO and LAO/STO, respectively, as the growth temperature is decreased from 800 to 700 °C. On increasing the growth temperature the activation energy increases from ~2 to 11 meV and ~7 to 20 meV in the high-temperature regime for LTO and LAO, respectively, and remains ~1 meV in the low-temperature region, while the value of exponent β is almost unaffected by growth temperature and varies from 0.2 to 0.8 throughout the temperature region.

The behavior of the photoconductivity decay in the oxide heterostructures appears quite similar to that seen in the $Ga_{0.3}Al_{0.7}As$,[42] $Ga_{0.8}Al_{0.2}N$,[35] and $Zn_{0.04}Cd_{0.96}Te$,[44] systems. The activation energy reported for these systems falls in the range of ~300 to 100 meV, which is one order higher in magnitude when compared to the LTO/STO and LAO/STO systems (10–20 meV). In general, smaller activation energies point to weak lattice relaxation.[45] Here, we note that the major factors that govern the relaxation effects in $Ga_{1-x}Al_xAs$ and oxide heterostructures are different. In $Ga_{1-x}Al_xAs$ and related systems, the local relaxation fundamentally stems from strain effects due to ionic size mismatch,[46,47] while in oxide heterostructures the origin is due to polar catastrophe. Thus, the low activation energies in the LTO/STO and LAO/STO heterostructures suggest that the intrinsic electric-field-induced redistribution of electronic states, due to the polar discontinuity, across the interface is rather weakly coupled to the lattice, thereby leading to small activation energies. However, the increase in the activation energy for the high-temperature-grown heterostructures may be attributed to the creation of oxygen vacancies, which couple strongly to the lattice.

D. Effect of electric field on optical response

It was shown earlier that the electrical conductivity of these structures can be modulated significantly by applying an electric field.[17,27,30] Here we examine the temporal dependence of this effect in order to compare it with the time evolution of the photoconducting state. Figures 5(a) and 5(b) show

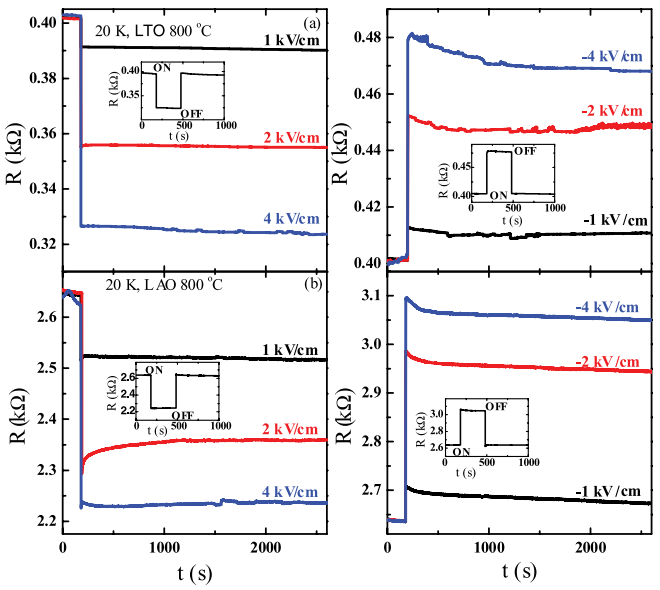

FIG. 5. (Color online) (a) and (b) Effect of ± gate field at 20 K on the LTO/STO and LAO/STO thin films fabricated in three-terminal configuration. After switching on the field the resistance is measured as a function of time. The effect of the gate field on the conductivity of the channel is much faster as compared to the effect of photoexcitation. A positive field makes the channel conducting while negative makes it more resistive. The effect of successive on and off cycles is shown in the insets.

the effects of a gate field E_g of ± 1, 2, and 4 kV/cm on these systems, which was applied in a back gate geometry. The channel resistance drops spontaneously on application of $+E_g$ and remains constant in time as long as the gate field is on. The system recovers quickly on a less than millisecond time scale on turning off the field. The effect of a negative gate field is to increase the resistance of the channel. However, the response time remains the same as seen for $+E_g$. The current-voltage curves of the channel for both polarities of the field remain Ohmic throughout the field range. The percentage change in channel resistance, defined as $\Delta R = \frac{|R(0)-R(E_g)|}{R(0)} \times 100$, for LTO and LAO at $E_g = 4$ kV/cm is 19.21 and 15.55, respectively. The dramatically different time dependence of ΔR seen during recovery from the photoexcitation and gating processes strongly suggests that these two fields act on different types of carrier. In order to arrive at a definite conclusion on this issue, we have done experiments in which the photon and electrostatic fields are applied in tandem.

Figure 6 shows the drop in resistance of the LTO and LAO heterostructures on photo exposure at 20 K. The samples were subjected to $\pm E_g$ during recovery 0, 100, 500, 1000, and 1500 s after turning off the light. An abrupt change in resistance takes

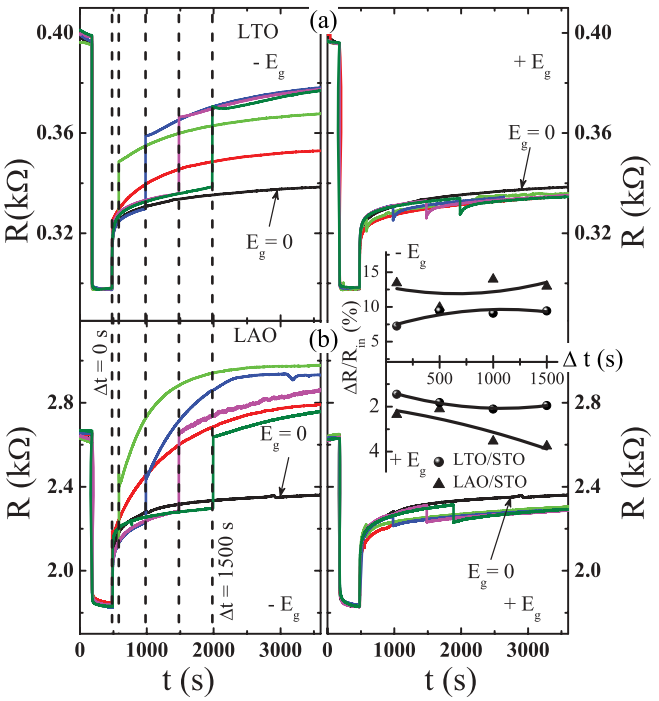

FIG. 6. (Color online) The combined effect of photo exposure and gate field ± 2 kV/cm on (a) LTO/STO and (b) LAO/STO at 20 K. The field is applied after certain time intervals (dotted lines, $\Delta t = 0$, 100, 500, 1000, and 1500 s) during the recovery of the system after extinguishing the photo exposure. The recovery of the resistance with an applied gate field is shown for the sake of comparison. It is clear that the negative field causes an abrupt and significant increase, whereas the effect of the positive field is small but still abrupt. The inset shows the relative change in the resistance ($\Delta R/R_{\text{in}}$) at the time when the gate field is applied. Here $\Delta R = |R_{\text{in}} - R_{\text{final}}|$ and the X axis is the time at which the field was turned on after terminating the photo exposure.

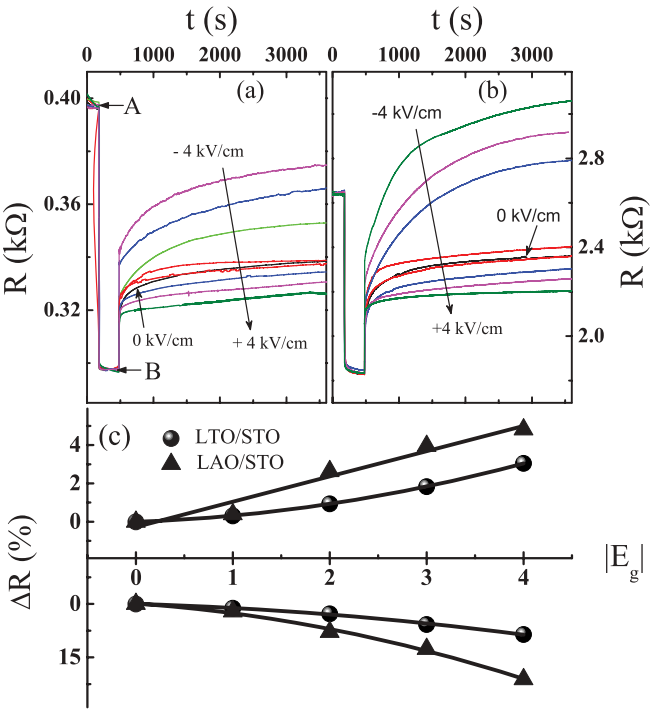

FIG. 7. (Color online) Recovery to the initial state under applied gate fields immediately after terminating the light exposure. (a) and (b) are for LTO/STO and LAO/STO, respectively, grown at 800 °C. The change in resistance (ΔR) at $t = 1000$ s as a function of gate field is shown in (c). At point A, shown in (a), the photo exposure with ~ 8 μW/cm^2 light is irradiated, while at point B the exposure is stopped and the system recovery is monitored as a function of time under different gate fields applied at the instant B. It can be clearly seen that fields of both polarities alter the recovery process; the conducting state of the system is arrested when $+E_g$ is applied and the recovery of higher resistibly is accelerated with $-E_g$.

place on application of the gate field. The resistance drops with $+E_g$ whereas it rises with $-E_g$. In the inset of Fig. 6 we plot the instantaneous change in R on application of $\pm E_g$ at several instants of time. The data show that the change in R due to the electric field is nearly independent of the state of recovery of the photoconducting state. This confirms our earlier observation that the two fields act on two different sources of carrier.

The recovery of the system from the photoconducting state at several values of the gate voltage is shown in Figs. 7(a) and 7(b) for LTO and LAO, respectively. The gate field was applied at the same time as the light was turned off. We clearly see that the recovery is accelerated by $-E_g$ whereas $+E_g$ slows it down. In the case of LAO/STO we also note that the negative field actually pushes the resistance beyond the value in the dark. In Fig. 7(c) we plot the change in resistance ΔR 1000 s after the application of the gate field. Here ΔR is defined as $\Delta R = \frac{|R(1000)_{E_g=0} - R(1000)_{E_g}|}{R(1000)_{E_g=0}}$.

E. Electronic structure and optical conductivity

To address the wavelength dependence of the photocurrent and to explain the decay of the photoexcited carriers, we study the band structure of the structurally relaxed LAO/STO

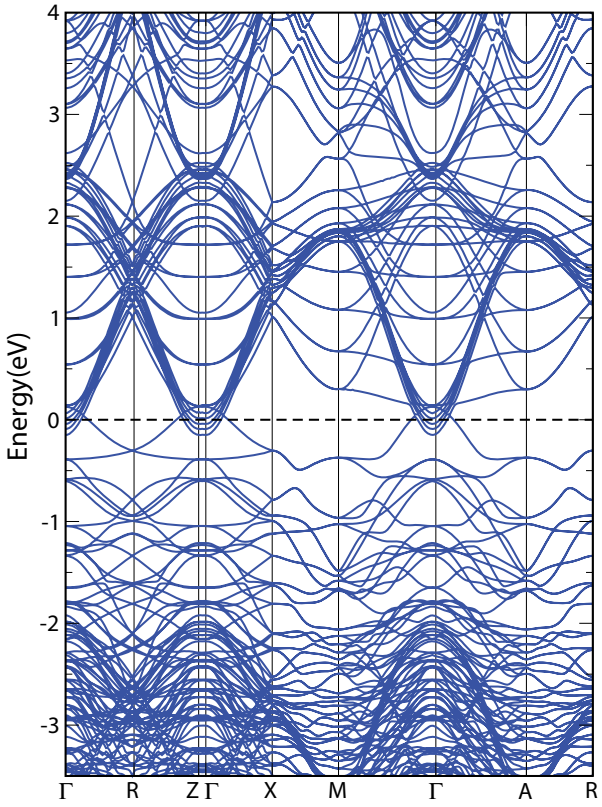

FIG. 8. (Color online) The FP-LAPW-generated band structure of the fully relaxed $LaAlO_3$-$SrTiO_3$ heterostructure. The zero on the energy scale represents the Fermi energy.

system. With the GGA formalism, the energy gap of the TiO_2-terminated $SrTiO_3$ was found to be 0.81 eV, while with two and three LAO layers the energy gap was reduced to 0.71 and 0.02 eV, respectively. For four unit cells of LAO on a TiO_2-terminated STO substrate the ground state was found to be metallic.

In Fig. 8, we show the ground state of a fully relaxed $(2 \times 2 \times 9)$-dimensional supercell with four units of LAO on TiO_2-terminated STO. In comparison with semiconductor heterostructures such as the AlGaAs/GaAs system, which also consists of two electronically gapped compounds sharing a common anion element, the valence-band wave functions in both LAO/STO and AlGaAs/GaAs heterostructures are seen to evolve mainly from the atomic wave function of the anions, while the conduction-band wave functions evolve mainly from the atomic wave functions of the cations. In the case of LAO/STO systems, there are few bands crossing the Fermi energy (E_F). The metallicity is due to the overlap of the surface O $2p$ bands of the AlO_2 layer with the Ti $3d$ bands of the TiO_2 interface, which is consistent with previous reports.[48] Furthermore, analysis of the band character shows that the states below E_F emanate mainly from O $2p$ orbitals. The tops of the valence bands are primarily composed of O $2p$ states resulting from the AlO_2 layers of the LAO film. With increasing energy and for $E - E_F > 2$ eV, we find that the states that constitute the band structure are essentially O $2p$ states of the TiO_2 layers of the STO motif. In other words, we find that the valence band of the LAO/STO system depicts a hierarchy in the distribution of O $2p$ states as a function of increasing binding energy, with widely distributed O $2p$ states of the AlO_2 layers forming the upper valence states ($E_F < E < -2$ eV), and those from the TiO_2 layers forming the intermediate valence bands which are relatively more localized over the energy range -2 eV $< E < -3$ eV.

On the other hand, the states above E_F are primarily composed of Ti $3d$ orbitals. Orbital decomposition of the states that constitute the bands crossing at E_F reveals that they are the t_{2g} states of Ti $3d$ orbitals of the TiO_2 interface, which are strongly hybridized with O $2p$ states of the surface AlO_2 layer. In the energy range $E_F < E < 2$ eV, the band structure traces a series of parallel sub-bands along the Brillouin zone edges. These are the $3d_{xy}$ bands of the Ti ions of the STO motif. The lowest of these parallel sub-bands emerges from the interfacial TiO_2 layer. With increasing energy in the unoccupied region of the band structure, these parallel sub-bands are found to emerge in succession from the $3d$ states of the TiO_2 layers of the STO motif, away from the interface. At $E \approx 2$ eV above E_F, one finds a conglomeration of Ti $3d$ bands of e_g character, localized over a very narrow energy interval. This localization of the e_g states is quite evident in the density of states spectrum as shown in Fig. 9(a).

From the band structure, we see that the number of bands crossing E_F are small, while there is a bunching of bands $\approx$2 eV above and below E_F. Therefore, one may expect that photoconductivity (PC) which results from interband transitions will occur between these states and the states at E_F, i.e., corresponding to wavelengths below 500 nm. Experimentally, this is observed for $\lambda < 440$ nm. Thus, in order to substantiate our arguments, we have calculated the

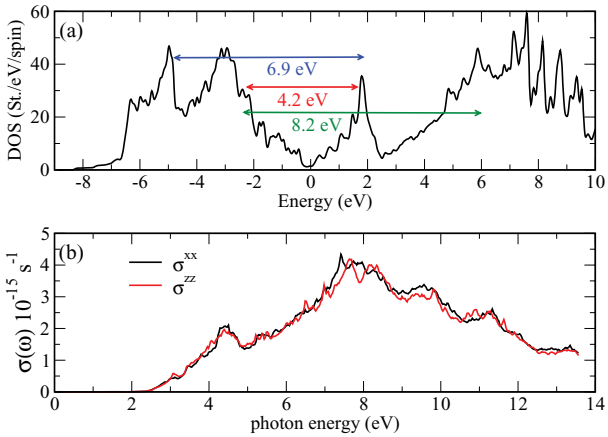

FIG. 9. (Color online) Total density of states (DOS) of the fully relaxed LAO/STO heterostructure, generated by density functional theory, showing the most probable transitions that can take place between the valence and conduction bands, and (b) optical conductivity $[\sigma(\omega)]$ for the two polarizations corresponding to the electric field in the basal plane (xx component) and along the c axis (zz component). For $E < 2.5$ eV, $\sigma(\omega)$ is small. It becomes significantly larger for $E > 2.5$ eV ($\lambda \approx 500$ nm), which is consistent with the experimental data where only a small intensity is observed for $\lambda > 440$ nm. Note that there is a reasonably good agreement between the transition energies shown in (a) and the $\sigma(\omega)$ peak positions shown in (b).

conductivity $\sigma(\omega)$ using Eqs. (1) and (2) from Ref. 49, for which the imaginary part of the dielectric function arising from interband transitions is given as

$$\epsilon_2^{\alpha}(\omega) = \frac{4\pi^2 e^2}{m^2\omega^2} \sum_{v,c} \frac{2}{V} \sum |\langle \psi_{c,k}|p_{\alpha}|\psi_{v,k}\rangle|^2 \delta\left[E_c(k) - E_v(k) - \hbar\omega\right], \quad (1)$$

where $\alpha = (x,y,z)$ is the axis index of the tetragonal cell, υ and c represents the valence and conduction band, respectively, and V is the supercell volume including the vacuum region. The optical conductivity $\sigma(\omega)$ is given as

$$\sigma(\omega) = \frac{\omega\epsilon_2(\omega)}{4\pi}. \quad (2)$$

The calculated $\sigma(\omega)$ is shown in Fig. 9(b). We find that for $E < 2.5$ eV, $\sigma(\omega)$ is small, and it becomes significantly larger for $E > 2.5$ eV ($\lambda \approx 500$ nm). This is consistent with the experimental data where only a small photoconductivity is observed for $\lambda > 440$ nm. Also, one may note that the mean-field nature of density functional theory limits the accuracy of band positions, and thus we expect a certain degree of uncertainty in the location of peaks in the calculated optical properties. Our calculations also find that there exist a number of peaks in $\sigma(\omega)$ located at around 4.4, 7.5, 9.5, and 11.3 eV. Peaks in $\sigma(\omega)$ arise from transitions involving parallel bands. These can be identified from the band structure (Fig. 8) or from the density of states [Fig. 9(a)]. We have shown in Fig. 9(a) the possible transitions which could lead to the 4.4 and 7.5 eV peaks in $\sigma(\omega)$. We mention that this is only indicative as the correct structure is obtained from the calculations based on Eqs. (1) and (2). We have calculated $\sigma(\omega)$ for the two polarizations corresponding to the electric field in the basal plane (xx component) and along the c axis (zz component). The anisotropy is very small, reminiscent of the pristine cubic structures of LAO and STO. There is a reasonably good agreement between the transition energies shown in Fig. 9(a) and the peak positions as shown in Fig. 9(b).

For both LAO/STO and LTO/STO heterostructures, the recovery from the UV radiation field photoconducting state follows a stretched exponential decay. The overall nature of the decay seems to be independent of the film growth conditions on the TiO_2-terminated STO. For low-carrier-density systems, such as for films grown at lower temperatures, the interface is atomically abrupt, thus being devoid of vacancy-induced states to act as traps. Thus, we argue that the source of the such trapping centers in oxide heterostructures is the closely spaced Ti $3d_{xy}$ bands. As seen from the band diagram of Fig. 8 for LAO/STO systems, the Ti $3d_{xy}$ states form flat parallel bands above E_F. Thus, according to the uncertainty principle $\Delta\epsilon\Delta t \geqslant \hbar$, where $\Delta\epsilon$ represents the bandwidth and Δt the carrier lifetime, it may be argued that for highly localized Ti $3d_{xy}$ states, the electrons trapped in these states would have a longer lifetime, resulting in a slower decay.

However, in comparison with LAO/STO, the LTO/STO systems show a larger decay constant. This may be partly attributed to the strong oxidation tendency of the $LaTiO_3$ which takes in oxygen from the interfacial layers of the STO substrate. It has been reported before that O vacancies in dilute concentrations will create new states in the band gap of $SrTiO_3$ below the conduction band,[50–52] representing a shallow state. These defect-induced states are also localized and may act as additional traps for the photoexcited carriers. Thus, one would expect that LTO/STO and also those systems which have been synthesized at higher temperatures that carry vacancies would have higher decay rates.

The sudden decrease in the photoconductivity on application of a gate voltage can also be reasonably well accounted for on the basis of the band picture. The excited states (conduction-band states) of these oxide heterostructures are derived from the Ti $3d$ states of the STO motif, which is an incipient ferroelectric. It has been previously shown that $SrTiO_3$ displays ferroelectric characteristics at low temperatures as well when subjected to strain and an external electric field.[53–55] Following the d^0-ness model, which explains the ferroelectric properties of the isoelectronic $BaTiO_3$ systems,[56,57] one may then expect an off-centering of the Ti ions in the first few layers of the substrate STO. Under these circumstances, changes in the Ti-O hybridization can therefore lead to dispersive bands. We expect that on application of an electric field the parallel Ti $3d_{xy}$ sub-bands, which act as trapping centers due to their localized nature, will be broadened and the carrier lifetime in these bands will be decreased.

IV. SUMMARY AND CONCLUSIONS

In summary, we have performed a comparative study of electronic transport in LTO/STO and LAO/STO heterostructures under the influence of radiation and electric fields, applied both separately and simultaneously. The heterostructures are found to be sensitive to near-ultraviolet radiation, which is well supported by optical calculations based on band theory. Both the systems show persistent photoconductivity, which follows a stretched exponential behavior. The difference in the energy scale for recovery in two temperature regions suggests a change in the migration dynamics of photoexcited carriers with the thermal energy available to the system. It is also pointed out that the change in resistance due to an electric field is almost independent of the state of recovery of the photoconducting state, which confirms that the two fields act on two different sets of carriers. The observed photoresponse is large for LTO/STO and is greatly affected by the growth temperature, i.e., it is higher for films grown at higher temperatures, thus suggesting a role for the oxygen vacancies created in STO during the film deposition. We argue that these localized vacancy states act like additional trap states for the carriers, thereby inducing the slow relaxation. However, the primary factor that governs the photocurrent decay is the Ti-derived $3d_{xy}$ states, which in the lower conduction band are highly localized. Following the uncertainty principle, localization of states lead to increased carrier lifetimes, and thus carriers trapped in these Ti $3d_{xy}$ states are expected to have longer lifetimes resulting in a slower decay. Thus, the relaxation dynamics of the charge carriers seems to be associated with the intrinsic properties of the $SrTiO_3$ substrates in these heterostructures.

ACKNOWLEDGMENTS

A.R. would like to acknowledge the Council of Scientific and Industrial Research (CSIR), India and Indian Institute of Technology Kanpur for financial support. R.C.B. acknowledges financial support from a J. C. Bose National Fellowship of the Department of Science and Technology, Government of India.

*rcb@nplindia.org

[1] A. Ohtomo and H. Y. Hwang, Nature (London) **427**, 423 (2004).
[2] G. S. Bhalla, C. Bell, J. Ravichandran, W. Siemons, Y. Hikita, S. Salahuddin, A. F. Hebard, H. Y. Hwang, and R. Ramesh, Nat. Phys. **7**, 80 (2011).
[3] S. Okamoto, A. J. Millis, and N. A. Spaldin, Phys. Rev. Lett. **97**, 056802 (2006).
[4] S. Okamoto and A. J. Millis, Nature (London) **428**, 630 (2004).
[5] R. Hesper, L. H. Tjeng, A. Heeres, and G. A. Sawatzky, Phys. Rev. B **62**, 16046 (2000).
[6] A. Ohtomo, A. D. Muller, J. L. Grazul, and H. Y. Hwang, Nature (London) **419**, 378 (2002).
[7] Y. Tokura, Y. Taguchi, Y. Okada, Y. Fujishima, T. Arima, K. Kumagai, and Y. Iye, Phys. Rev. Lett. **70**, 2126 (1993).
[8] W. Siemons, G. Koster, H. Yamamoto, W. A. Harrison, G. Lucovsky, T. H. Geballe, D. H. A. Blank, and M. R. Beasley, Phys. Rev. Lett. **98**, 196802 (2007).
[9] A. Kalabukhov, R. Gunnarsson, J. Börjesson, E. Olsson, T. Claeson, and D. Winkler, Phys. Rev. B **75**, 121404 (2007).
[10] A. Ohtomo and H. Y. Hwang, Nature (London) **441**, 120 (2006).
[11] A. D. Caviglia, S. Gariglio, C. Cancellieri, B. Sacépé, A. Fête, N. Reyren, M. Gabay, A. F. Morpurgo, and J.-M. Triscone, Phys. Rev. Lett. **105**, 236802 (2010).
[12] M. Huijben, G. Rijnders, D. H. A. Blank, S. Bals, S. Van Aert, J. Verbeeck, G. Van Tendeloo, A. Brinkman, and H. Hilgenkamp, Nat. Mater. **5**, 556 (2006).
[13] D. A. Dikin, M. Mehta, C. W. Bark, C. M. Folkman, C. B. Eom, and V. Chandrasekhar, Phys. Rev. Lett. **107**, 056802 (2011).
[14] Lu Li, C. Richter, J. Mannhart, and R. C. Ashoori, Nat. Phys. **7**, 762 (2011).
[15] A. Brinkman, M. Huijben, M. van Zalk, J. Huijben, U. Zeitler, J. C. Maan, W. G. van der Wiel, G. Rijnders, D. H. A. Blank, and H. Hilgenkamp, Nat. Mater. **6**, 493 (2007).
[16] G. Herranz, M. Basletić, M. Bibes, C. Carrétéro, E. Tafra, E. Jacquet, K. Bouzehouane, C. Deranlot, A. Hamzić, J.-M. Broto, A. Barthélémy, and A. Fert, Phys. Rev. Lett. **98**, 216803 (2007).
[17] S. Thiel, G. Hammerl, A. Schmehl, C. W. Schneider, and J. Mannhart, Science **313**, 1942 (2006).
[18] J. Biscaras, N. Bergeal, A. Kushwaha, T. Wolf, A. Rastogi, R. C. Budhani, and J. Lesueur, Nat. Commun. **1**, 89 (2010).
[19] R. Pentcheva, M. Huijben, K. Otte, W. E. Pickett, J. E. Kleibeuker, J. Huijben, H. Boschker, D. Kockmann, W. Siemons, G. Koster, H. J. W. Zandvliet, G. Rijnders, D. H. A. Blank, H. Hilgenkamp, and A. Brinkman, Phys. Rev. Lett. **104**, 166804 (2010).
[20] Z. S. Popović, S. Satpathy, and R. M. Martin, Phys. Rev. Lett. **101**, 256801 (2008).
[21] R. Pentcheva and W. E. Pickett, J. Phys.: Condens. Matter **22**, 043001 (2010).
[22] J. Biscaras, N. Bergeal, S. Hurand, C. Grossetête, A. Rastogi, R. C. Budhani, D. LeBoeuf, C. Proust, and J. Lesueur, Phys. Rev. Lett. **108**, 247004 (2012).
[23] W.-J. Son, E. Cho, B. Lee, J. Lee, and S. Han, Phys. Rev. B **79**, 245411 (2009).
[24] Y. Kozuka, T. Susaki, and H. Y. Hwang, Phys. Rev. Lett. **101**, 096601 (2008).
[25] S. S. A. Seo, Z. Marton, W. S. Choi, G. W. J. Hassink, D. H. A. Blank, H. Y. Hwang, T. W. Noh, T. Egami, and H. N. Lee, Appl. Phys. Lett. **95**, 082107 (2009).
[26] C. H. Ahn, J.-M. Triscone, and J. Mannhart, Nature (London) **424**, 1015 (2003).
[27] N. Reyren, S. Thiel, A. D. Caviglia, L. Fitting Kourkoutis, G. Hammerl, C. Richter, C. W. Schneider, T. Kopp, A.-S. Ruetschi, D. Jaccard, M. Gabay, D. A. Muller, J.-M. Triscone, and J. Mannhart, Science **317**, 1196 (2007).
[28] C. Cen, S. Thiel, G. Hammerl, C. W. Schneider, K. E. Andersen, C. S. Hellberg, J. Mannhart, and J. Levy, Nat. Mater. **7**, 298 (2008).
[29] K. Ueno, S. Nakamura, H. Shimotani, A. Ohtomo, N. Kimura, T. Nojima, H. Aoki, Y. Iwasa, and M. Kawasaki, Nat. Mater. **7**, 855 (2008).
[30] A. Rastogi, A. K. Kushwaha, T. Shiyani, A. Gangawar, and R. C. Budhani, Adv. Mater. **22**, 4448 (2010).
[31] A. Rastogi and R. C. Budhani, Opt. Lett. **37**, 317 (2012).
[32] H. L. Störmer, R. Dingle, A. C. Gossard, W. Wiegmann, and M. D. Sturge, Solid State Commun. **29**, 705 (1979).
[33] H. J. Queisser and D. E. Theodorou, Phys. Rev. B **33**, 4027 (1986).
[34] J. C. Fan, J. C. Wang, and Y. F. Chen, Appl. Phys. Lett. **75**, 2978 (1999).
[35] E. Arslan, S. Butun, S. B. Lisesivdin, M. Kasap, S. Ozcelik, and E. Ozbay, J. Appl. Phys. **103**, 103701 (2008).
[36] M. Lax, Phys. Rev. **119**, 1502 (1960).
[37] P. Blaha, K. Schwarz, G. Madsen, D. Kvasicka, and J. Luitz, computer code WIEN2K, Technical University of Vienna, Vienna, 2001.
[38] R. Kohlrausch, Ann. Phys. (Leipzig) **12**, 393 (1847).
[39] R. G. Palmer, D. L. Stein, E. Abrahams, and P. W. Anderson, Phys. Rev. Lett. **53**, 958 (1984).
[40] R. V. Chamberlin, G. Mozurkewich, and R. Orbach, Phys. Rev. Lett. **52**, 867 (1984).
[41] D. V. Lang and R. A. Logan, Phys. Rev. Lett. **39**, 635 (1977).
[42] J. Y. Lin, A. Dissanayake, G. Brown, and H. X. Jiang, Phys. Rev. B **42**, 5855 (1990).
[43] C. H. Henry and D. V. Lang, Phys. Rev. B **15**, 989 (1977).
[44] A. S. Dissanayake, J. Y. Lin, and H. X. Jiang, Phys. Rev. B **48**, 8145 (1993).
[45] B. A. S. Dissanayake and H. X. Jiang, Appl. Phys. Lett. **61**, 2048 (1992).
[46] D. J. Chadi and K. J. Chang, Phys. Rev. Lett. **61**, 873 (1988).
[47] P. M. Mooney, J. Appl. Phys. **67**, R1 (1990).
[48] R. Pentcheva and W. E. Pickett, Phys. Rev. Lett. **102**, 107602 (2009).
[49] L. Dorigoni, O. Bisi, F. Bernardini, and S. Ossicini, Phys. Rev. B **53**, 4557 (1996).

[50]D. Ricci, G. Bano, G. Pacchioni, and F. Illas, Phys. Rev. B **68**, 224105 (2003).
[51]S. Kimura, J. Yamauchi, M. Tsukada, and S. Watanabe, Phys. Rev. B **51**, 11049 (1995).
[52]C. Lee, J. Destry, and J. L. Brebner, Phys. Rev. B **11**, 2299 (1975).
[53]J. H. Haeni, P. Irvin, W. Chang, R. Uecker, P. Reiche, Y. L. Li, S. Choudhury, W. Tian, M. E. Hawley, B. Craigo, A. K. Tagantsev, X. Q. Pan, S. K. Streiffer, L. Q. Chen, S. W. Kirchoefer, J. Levy, and D. G. Schlom, Nature (London) **430**, 758 (2004).
[54]O. Tikhomirov, H. Jiang, and J. Levy, Phys. Rev. Lett. **89**, 147601 (2002).
[55]E. Hegenbarth, Phys. Status Solidi **6**, 333 (1964).
[56]R. E. Cohen, Nature (London) **358**, 136 (1992).
[57]N. A. Hill, J. Phys. Chem. B **104**, 6694 (2000).